

Hadroproduction of φ -mesons in the Quark-Gluon String model

G.H. Arakelyan¹, C. Merino², and Yu.M. Shabelski³

¹A.Alikhanyan National Scientific Laboratory
(Yerevan Physics Institut)
Yerevan, 0036, Armenia
e-mail: argev@mail.yerphi.am

²Departamento de Física de Partículas, Facultade de Física
and Instituto Galego de Física de Altas Enerxías (IGFAE)
Universidade de Santiago de Compostela Santiago de Compostela 15782
Galiza-Spain
e-mail: merino@fpaxpl.usc.es

³Petersburg Nuclear Physics Institute
NCR Kurchatov Institute
Gatchina, St.Petersburg 188350, Russia
e-mail: shabelsk@thd.pnpi.spb.ru

Abstract

We consider the experimental data on φ -meson production in hadron-nucleon collisions for a wide energy region. The Quark-Gluon String Model quantitatively describes the spectra of secondary φ , as well as the ratios of φ/π^- and φ/K^- production cross sections.

PACS. 25.75.Dw Particle and resonance production

1 Introduction

The Quark-Gluon String Model (QGSM) [1, 2], based on the Dual Topological Unitarization (DTU), Regge phenomenology, and nonperturbative notions of QCD, has been for already more than thirty years to successfully predict and describe many features of the hadronic processes in a wide energy range. In particular, the QGSM allows one to make quantitative predictions on the inclusive densities of different secondaries both in the central and beam fragmentation regions.

In the QGSM frame, high energy hadron-nucleon collisions are considered as taking place via the exchange of one or several Pomerons. Each Pomeron is considered in DTU as a cylindrical diagram (Fig. 1a). The cut [3] between Pomerons in a multipomeron diagram results in elastic or diffraction dissociation processes, while the cut through one (Fig. 1b) or several (Fig. 1c) Pomerons corresponds to inelastic processes with multiple production of secondaries, the cut of every Pomeron leading to the production of two showers of secondaries.

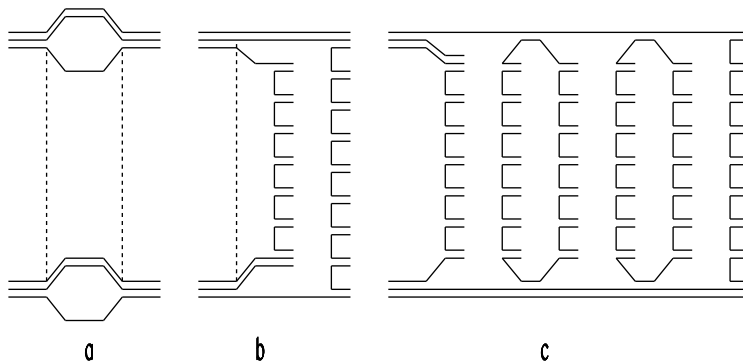


Figure 1: (a) Cylindrical diagram representing a Pomeron exchange within the DTU classification (quarks are shown by solid lines); (b) A cut of the cylindrical diagram corresponding to the single-Pomeron exchange contribution to inelastic pp scattering; (c) The cuts of the diagrams for the inelastic interaction of the incident proton with a target nucleon in a pp collision.

This model has been successfully used for the description of multiparticle production processes in hadron-hadron collisions. The QGSM description of the production of secondaries (pseudoscalar mesons π and K), and of nucleons p , \bar{p} , which give the main contribution to mean multiplicity at different energies was obtained many years ago in [4, 5] (see also [6, 7]). Vector meson production was considered in [8, 9, 10]. The yields of hyperons, including the multistrange ones, has been described in [11, 12].

In the present paper, we apply first time the QGSM formalism to the description of the spectra of vector φ -mesons production in πp and pp collisions, and of the ratios of yields φ/π^- and φ/K^- in pp -collisions for a large scope of the initial energy going up to the RHIC and LHC ranges. The φ -meson is a system, of $s\bar{s}$ quarks with non-zero masses, that is rarely produced, and that it can be thus sensitive to the production mechanism.

2 Meson production in the QGSM

In the QGSM the inclusive spectrum of a secondary hadron h is determined [1, 2] by the convolution of the diquark, valence quark, and sea quark distributions, $u(x, n)$, in the incident particles, with the fragmentation functions, $G^h(z)$, of quarks and diquarks into the secondary hadron h . Both the distribution and the fragmentation functions are constructed using the Reggeon counting rules [13].

For a nucleon target, the inclusive rapidity, y , or Feynman- x , x_F , spectrum of a secondary hadron h has the form [1]:

$$\frac{dn}{dy} = \frac{x_E}{\sigma_{inel}} \cdot \frac{d\sigma}{dx_F} = \sum_{n=1}^{\infty} w_n \cdot \phi_n^h(x) + w_D \cdot \phi_D^h(x) , \quad (1)$$

where the functions $\phi_n^h(x)$ determine the contribution of diagrams with n cut Pomerons, w_n is the relative weight of this diagram, that it depends on the beam particle, and the term $w_D \cdot \phi_D^h(x)$ accounts for the contribution of diffraction dissociation processes.

In the case of pp collisions:

$$\begin{aligned} \phi_n^h(x) &= f_{qq}^h(x_+, n) \cdot f_q^h(x_-, n) + f_q^h(x_+, n) \cdot f_{qq}^h(x_-, n) \\ &+ 2(n-1) \cdot f_s^h(x_+, n) \cdot f_s^h(x_-, n) , \end{aligned} \quad (2)$$

$$x_{\pm} = \frac{1}{2} [\sqrt{4m_T^2/s + x^2} \pm x] , \quad (3)$$

where f_{qq} , f_q , and f_s correspond to the contributions of diquarks, valence quarks, and sea quarks, respectively.

In the case of meson-nucleon collisions, the diquark contribution $f_{qq}^h(x_+, n)$ in Eq. (2) should be replaced by the valence antiquark contributions $f_{\bar{q}}^h(x_+, n)$. Thus, in the case of meson-nucleon collisions, the quark and antiquark contributions would be determined, respectively, by the convolution of the quark and antiquark distributions with the corresponding fragmentation functions, e.g.

$$f_q^h(x_+, n) = \int_{x_+}^1 u_q(x_1, n) \cdot G_q^h(x_+/x_1) dx_1 . \quad (4)$$

The details of the model are presented in [1, 2, 4, 5, 11], and we use in this paper the Pomeron parameters in ref. [5].

The averaged number of exchanged Pomerons in pp collisions $\langle n \rangle_{pp}$ slowly increases with the energy. In particular, in the case of $n > 1$, i.e. in the case of multipomeron exchange, the distributions of valence quarks and diquarks are softened due to the appearance of a sea quark contribution [14].

The production of π and K mesons in pp collisions, starting from comparatively low energies, was analyzed in [4, 5].

For the φ -meson production we use the following quark fragmentation functions [8]:

$$G_u^\varphi = G_d^\varphi = a_\varphi \cdot (1-z)^{\lambda-\alpha_R-2\alpha_\varphi+2}, \quad (5)$$

$$G_s^\varphi = a_\varphi \cdot (1-z)^{\lambda-\alpha_\varphi}. \quad (6)$$

On the other hand, the diquark fragmentation functions into φ -mesons have the form:

$$G_{uu}^\varphi = G_{ud}^\varphi = a_\varphi \cdot (1-z)^{\lambda+\alpha_R-2(\alpha_R+\alpha_\varphi)}, \quad (7)$$

where the parameter λ takes the value $\lambda=0.5$ [1, 4, 5], and the parameters $\alpha_R=0.5$ and $\alpha_\varphi=0$. are the intercepts of the ρ and φ Regge trajectories, respectively. The value of the parameter a_φ is determined by comparison to experimental data on ϕ production from different hadron beams. In our calculations we use the value $a_\varphi = 0.11$.

3 Numerical results

In this section we compare the QGSM calculations to the experimental data on φ inclusive cross sections in πp [15, 16, 17] and pp [17, 18, 19, 20, 21] collisions at different energies, and to the experimental data on ratios of φ/π and φ/K [22, 23, 24] for energies up to the LHC range.

In Fig. 2 we compare two sets of experimental data for x_F -spectra of φ -mesons produced in $\pi^\pm p$ collisions for two different initial momenta of π -mesons, 93–140 GeV/c (upper panel) and 175–360 GeV/c (lower panel), measured by different collaborations [15, 16, 17, 19], to the corresponding QGSM calculations. The full curve on the upper panel was calculated at 140 GeV/c, while the full curve on the lower panel corresponds to momenta 200 GeV/c and the dashed curve to momenta 360 GeV/c.

As we can see on Fig.2, for πp -collision there is a remarkable disagreement between experimental data [15, 17] and [19], these being significantly higher. The data [15, 16, 17] were measured on proton target, while data [19] were measured on Be target, and the absolute cross section per nucleon have been obtained using linear A-dependence. As it was mentioned in [19], the origin of the difference in the normalization has not been found.

The theoretical QGSM curves for π^+ and π^- beams practically coincide.

The QGSM description of the experimental data on the x_F dependence of $d\sigma/dx_F$ -spectra of φ -mesons at pp -collision measured at different energies [16, 17, 18, 19] is presented in Fig. 3, where one can see that the difference between the normalisation of different experiments in pp collisions is not so large as for πp collisions. The full curve in Fig. 3 corresponds to the QGSM calculations at 158 GeV/c. Here, the agreement of the QGSM calculation with the experimental data [18] is remarkably good. For the determination of the normalisation parameter a_φ experimental results by [15, 16, 18] have been used.

In Fig. 4, we compare the QGSM calculations to the experimental data on the inclusive spectra $x_F \cdot d\sigma/dx_F$ of φ -mesons in pp -collisions at 400 GeV/c [20]. In Fig. 5,

the y -spectra dn/dy of φ -mesons production in pp -collisions at 400 GeV/c [20] are compared to the QGSM calculations at the same energy. The theoretical predictions for the same spectra at LHC energies 7 (dashed curve) and 14 TeV (dashed-dotted curve) are also presented.

As it is shown in Figs. 2 to 5, the QGSM description of the experimental data at intermediate energies is consistently satisfactory.

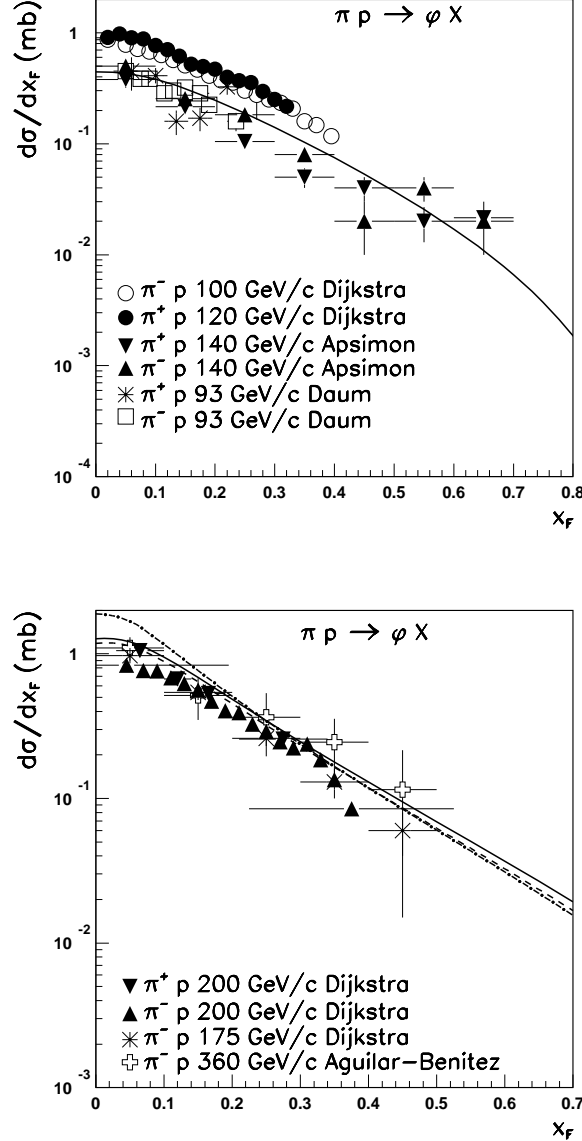


Figure 2: Two sets of experimental data on the x_F -spectra of φ -mesons produced in $\pi^\pm p$ collisions for two different initial momenta of π -mesons 93–140 GeV/c (upper panel) and 175–360 GeV/c (lower panel), measured by different collaborations [15, 16, 17, 19], and the corresponding theoretical curves (see the main text).

To calculate the φ/π and φ/K cross section ratios one needs the calculated values of both φ and pseudoscalar π and K -mesons cross sections. For π mesons the QGSM

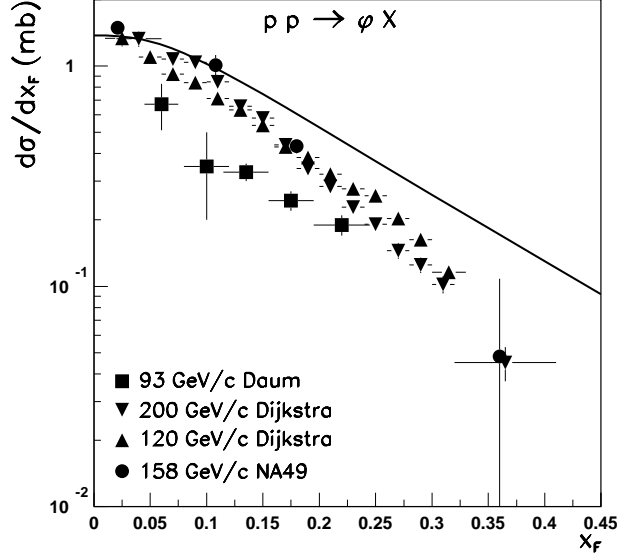


Figure 3: The experimental data on the x_F -spectra of φ -mesons produced in pp collisions at different energies [18, 19, 17], compared to the corresponding QGSMM calculation at 158 GeV/c (full curve).

predictions are rather reliable [4, 5, 7] up to the LHC energies, taking into account in Eq. (3) the growth of the $\langle p_T \rangle$ of produced π , K and φ - mesons with energy.

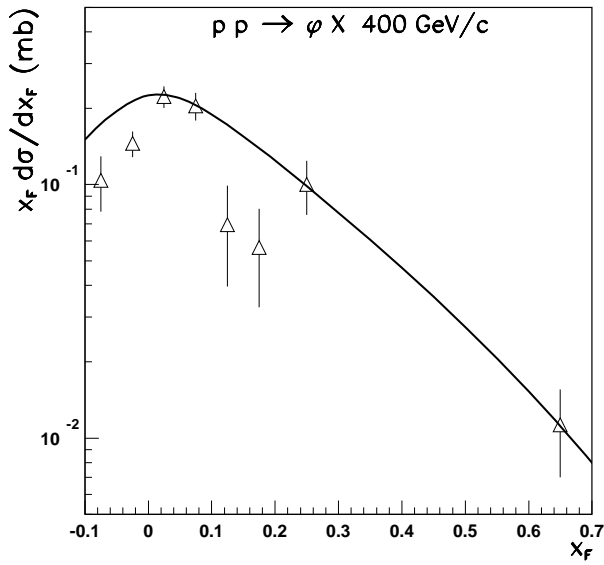


Figure 4: The experimental data on the x_F -spectra $x_F d\sigma/dx_F$ of φ -mesons produced in pp collisions at 400 GeV/c [20], compared to the corresponding QGSMM calculation.

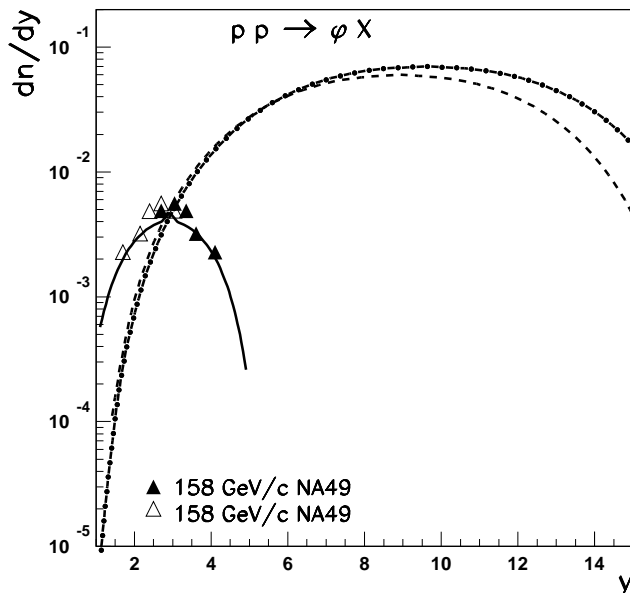


Figure 5: The experimental data [20] on the y -spectra dn/dy of φ -mesons produced in pp collisions at 158 GeV/c, and the corresponding QGSM result (full line). The QGSM predictions for LHC energies 7 (dashed line) and 14 TeV (dashed-dotted line) are also presented.

In Fig. 6 we present the QGSM description of the experimental data on the inclusive spectra of K^+ (upper panel) and K^- (lower panel) mesons in pp -collisions on a wide energy range, going from 100 GeV/c up to $\sqrt{s}=200$ GeV [18, 21]. The integrated over p_T RHIC data at $\sqrt{s}=200$ GeV have been taken from [18]. This data were obtained by the NA49 Collaboration in ref. [18] by interpolating the RHIC data at different p_T .

In Fig. 6 one can appreciate that at low energies the normalization of the experimental data at 100 and 175 GeV/c in ref. [21] differs from that of the experimental data in ref. [18] at 158 GeV/c. We present the results of the QGSM calculations at two different energies: 158 GeV/c ($\sqrt{s}=17.3$ GeV), by solid curves, and RHIC energy ($\sqrt{s}=200$ GeV), by dashed curves. One can see that the theoretical calculations at $\sqrt{s}=200$ GeV decrease alightly more rapidly than those at $\sqrt{s}=17.3$ GeV.

The energy dependence of the production cross section ratios of φ/π^- (upper panel) [22, 23] and ϕ/K^- (lower panel) [22, 24] in pp collisions are presented in Fig. 7, where the QGSM description is shown by solid curves. The shapes of the two theoretical curves are similar because the ratio of K/π production depends rather weakly on the initial energy. The discrepancies of the theoretical curves with the experimental points at high energies in Fig. 7 can be connected to the differences in the kinematical windows for φ , K , and π experimental measurements at LHC energies.

4 Conclusion

The QGSM provides a reasonable description of Feynman x_F and rapidity y spectra of φ -meson production for the interaction of different hadron beams with a nucleon target in a wide energy region, by only using one new normalization parameter, $a_\varphi=0.11$. We show the QGSM prediction for dn/dy cross sections for LHC energies. We have also obtained a reasonable agreement for the φ/π and φ/K cross section ratios in a wide interval of the beam energy, going up to the LHC range.

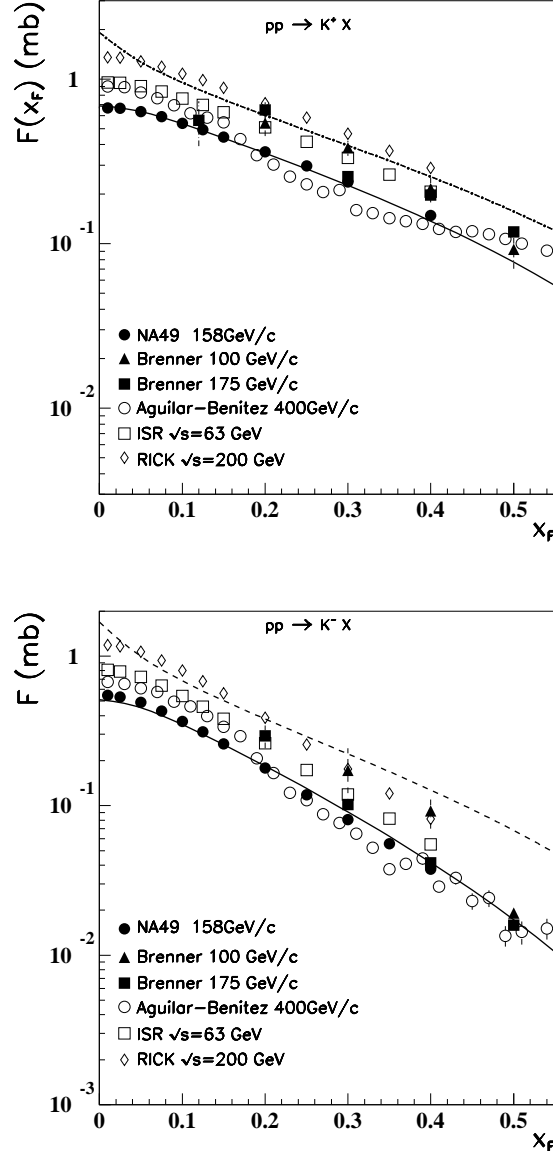


Figure 6: The QGSM description of the invariant cross section of K^+ (upper panel) and K^- (lower panel) mesons produced in pp collisions compared to the experimental data at different energies [18, 21]. Solid lines correspond to the QGSM result at 158 GeV/c ($\sqrt{s}=17.3$ GeV), while dashed lines correspond to the QGSM calculation at RHIC energy ($\sqrt{s}=200$ GeV).

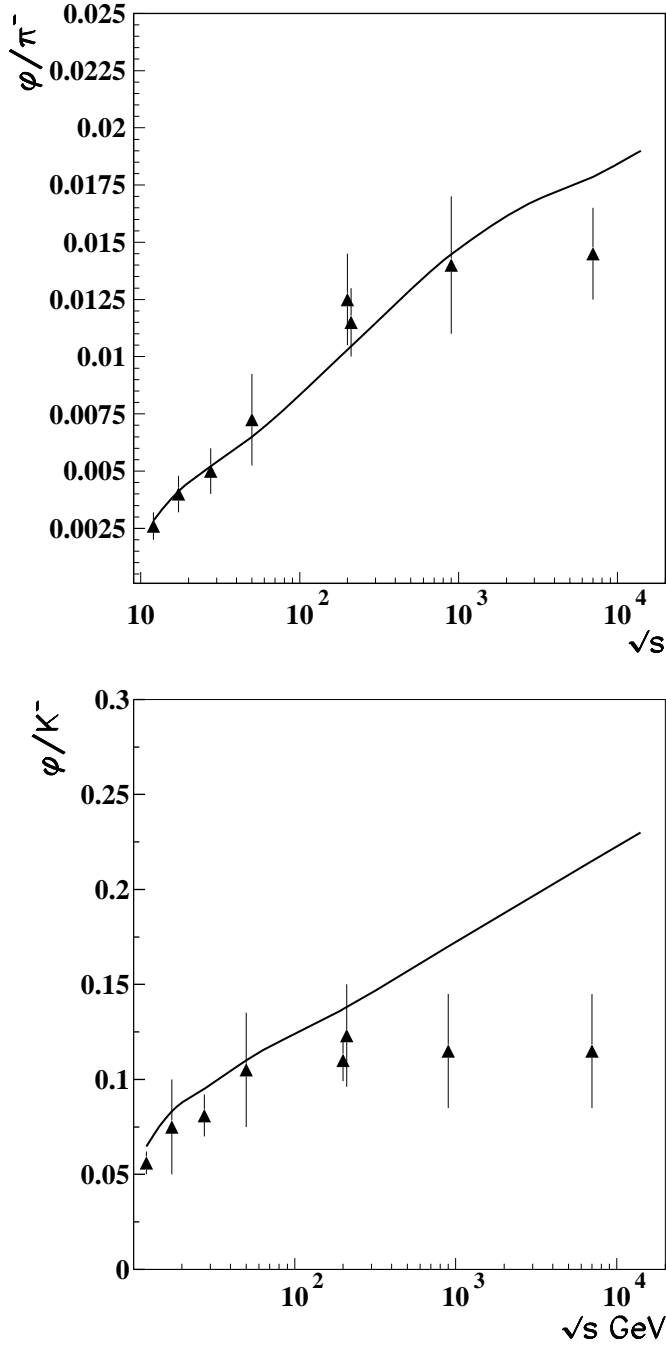


Figure 7: The QGSM description of the \sqrt{s} dependence of ϕ/π^- (upper panel) and ϕ/K^- (lower panel) cross section ratios produced in pp collisions, compared to the corresponding experimental data in refs. [22, 23, 24].

Acknowledgements

We thank C. Pajares for useful discussions. We are also grateful to N.I. Novikova for technical help. This paper was supported by Ministerio de Economía y Competitividad of Spain (FPA2011–22776), the Spanish Consolider-Ingenio 2010 Programme CPAN (CSD2007-00042), by Xunta de Galicia, Spain (2011/PC043), by the State Committee of Science of the Republic of Armenia (Grant-13-1C023), and, partially, by grant RSGSS-3628.2008.2.

References

- [1] A.B. Kaidalov and K.A. Ter-Martirosyan, *Yad. Fiz.* **39**, 1545 (1984); **40**, 211 (1984).
- [2] A.B. Kaidalov. *Phys. Atom. Nucl.*, **66**, 781 (2003).
- [3] V.A. Abramovsky, V.N. Gribov, and O.V. Kancheli, *Yad. Fiz.* **18**, 595 (1973).
- [4] A.B. Kaidalov and O.I. Piskounova, *Yad. Fiz.* **41**, 1278 (1985).
- [5] Yu.M. Shabelski, *Yad. Fiz.* **44**, 186 (1986).
- [6] G.H. Arakelyan, C. Merino, C. Pajares, and Yu.M. Shabelski, *Eur. Phys. J. C* **54**, 577 (2008) and hep-ph/0709.3174.
- [7] C. Merino, C. Pajares, and Yu.M. Shabelski, *Eur. Phys. J. C* **71**, 1652 (2011).
- [8] G.H. Arakelyan, Sh.S. Eremian. *Phys. Atom. Nucl.* **58**, 1241 (1995), *Yad. Fiz.* **58**, 132 (1995).
- [9] Sh.S. Eremian, *Phys. Atom. Nucl.* **59**, 144 (1996).
- [10] G.H. Arakelyan, C. Pajares, and Yu.M. Shabelski. *Z. Phys.* **C73**, 697 (1997) and hep-ph/9602348.
- [11] G.H. Arakelyan, A. Capella, A.B. Kaidalov, and Yu.M. Shabelski, *Eur. Phys. J. C* **26**, 81 (2002) and hep-ph/0103337.
- [12] G.H. Arakelyan, A.B. Kaidalov, C. Merino, and Yu.M. Shabelski, *Phys. Atom. Nucl.* **74**, 426 (2011), and arXiv:1004.4074[hep-ph].
- [13] A.B. Kaidalov, *Sov. J. Nucl. Phys.* **45**, 902 (1987).
- [14] A.B. Kaidalov, K.A. Ter-Martirosyan, and Yu.M. Shabelski, *Yad. Fiz.* **43**, 1282 (1986).
- [15] R.J. Apsimon *et al.*, Omega-Photon Collaboration, *Z. Phys.* **C61**, 383 (1994); F-D. Gebert, Bonn-IR-92-10 (1992).
- [16] M. Aguilar-Benitez *et al.*, LEBC-EHS Collaboration, *Z. Phys.* **C44**, 531 (1989).
- [17] C. Daum *et al.*, *Nucl. Phys.* **B186**, 205 (1981)
- [18] S.V. Afanasiev *et al.*, NA49 Collaboration, *Phys. Lett. B* **491**, 59 (2000); T. Anticic *et al.*, NA49 Collaboration, *Eur. Phys. J. C* **68**, 1 (2010).
- [19] H. Dijkstra *et al.*, ACCMOR Collaboration, *Z. Phys.* **C31**, 375 (1986).
- [20] M. Aguilar-Benitez *et al.*, LEBC-EHS Collaboration, *Z. Phys.* **C50**, 405 (1991).

- [21] A.E. Brenner *et al.*, Phys. Rev. D**26**, 1497 (1982).
- [22] J. Adams *et al.*, STAR Collaboration, Phys.Lett. **B 612**, 181 (2005) and nucl-ex/0406003.
- [23] B. Abelev *et al.*, ALICE Collaboration, Phys. Lett. B**710**, 557 (2012) and arXiv:1112.2082[hep-ex].
- [24] B. Abelev *et al.*, ALICE Collaboration, Eur. Phys. J. C**72**, 2183 (2012) and arXiv:1208.5717[hep-ex].